27

Spatial Dynamics of a Benthic Community: Applying Multiple Models to a Single System

Douglas Donalson, Robert A. Desharnais, Carlos D. Robles, and Roger Nisbet

CONTENTS

27.1 Introduction

Understanding the effects of spatial processes on population dynamics is essential to the advancement of the science of ecological modeling. Inclusion of spatial processes in a model can significantly alter the dynamic predictions made by nonspatial models. Although models that allow for spatial interactions can provide insights into ecological dynamics, there are difficulties as well. It can be difficult to deduce the relative importance of underlying mechanisms causing the altered dynamics from simulation results without the tools of mathematical analysis. Also, confirming that the computer code driving the model is working, is a nontrivial task. As additional complexity is added to increase realism of the model, these tasks increase in difficulty. Using different model types to represent the dynamics under study can provide both additional ways to test that models are working correctly and to better understand the various mechanisms contributing to the system dynamics.

When choosing a model for use in a research project, it is important to make sure that the model class can represent all the important dynamic interactions in the system. A model class can loosely be defined as a group of models that all have the same underlying structure. Within this grouping, models based on differential equations are a model class, as are all deterministic models. Model classes are often described along Holling's gradient with end points *strategic* (very general), such as ordinary differential equation models (ODE), and *tactical* (very specific), such as agent-based models (ABMs). However, this is not always an accurate way to partition different model classes. Instead, we look at the relative ease of design and analysis against the assumptions inherent in the structure of the model class. We use a sliding scale of simplicity to complexity of model class. At one end of the scale are models that are simple to design and analyze but have very restrictive assumptions; on the other end are models that are difficult to design and analyze but remove constraints of simple model classes.

A key to understanding the difference between model classes is recognition of implicit model assumptions. All models involve explicit and implicit assumptions. Explicit assumptions are the mechanisms chosen by the researcher to simulate the various dynamics involved in the system under study. These

0-8493-1344-9/04/$0.00+$1.50

are, for the most part, independent of the class of model used. Examples of these are logistic vs. exponential growth, and Type I, II, or III functional responses.[1]

Implicit model assumptions are those that characterize the model class. A good starting point for a discussion of implicit model assumptions are the Lotka-Volterra predator–prey equations. These are a well-known example of the ODE class of models. The two most significant implicit assumptions of the Lotka-Volterra models (and in fact, any ODE model) are, first, that the system is "well mixed," that all individuals are identical and all individuals experience identical conditions; and, second, that there are enough individuals that demographic stochasticity has minimal effect on the population dynamics. In natural systems, these two assumptions are usually mutually exclusive. Spatial scales small enough to guarantee a homogeneous environment can host only small populations and are therefore potentially subject to strong demographic stochasticity. Spatial scales that can maintain populations large enough to minimize demographic stochasticity are seldom homogeneous. The combination of these two assumptions in a single model can be restrictive.

How then can we determine what type of model class should be used for what situation? Choosing the model class at the beginning of the project on the basis of projected system dynamics is often not a good option. This is particularly true when dealing with potentially complex spatial processes where the interactions in time and space at different scales can cause the dynamics to deviate from linear predictions.[2–5] In contrast, using a complex spatial model to analyze basic system behavior such as potential equilibria and sensitivity analysis is seldom practical because of the slower speed of the simulations and the stochasticity inherent in the results. Therefore, we need some way to evaluate different models against the system we wish to simulate to ensure we are using the correct tools for the job.

In this chapter we describe four complementary model classes and their interrelations. We then introduce four models of an intertidal predator–prey system, each of which represents one of the four model classes. We use some of the results from our testing of the four models to demonstrate a few of the advantages of our multiple model approach. The focus of this chapter is on model comparisons; later work will attempt to match model results to natural systems.

27.2 Four Model Classes

The properties of the ODE class of models are well known. Aside from the implicit assumptions previously discussed, there are two important properties of ODEs for the purposes of this chapter. First, there are a wide range of analytical and numerical tools available that allow detailed analysis of the dynamics of the system. Second, simulations of ODE-based models are fast when compared to their more complex counterparts. Because of this, ODE models provide an excellent baseline for modeling projects.

The stochastic birth–death (SBD) model class removes the restriction that demographic stochasticity is negligible while still requiring that all spatial processes be "well mixed" and that all individuals are identical. We spend a bit more time on SBD models because they are powerful but seldom-used additions to the modeler's tool kit. SBD models are generally defined using an underlying deterministic model. To construct an SBD, two changes are made to the deterministic model. The first is that the state variables are constrained to integer values (but see the SBD model later in this chapter for a specific exception to this rule). This represents a more realistic view of populations, as changes in population size occur through loss or gain of individuals, not pieces of individuals. Second, the terms of the deterministic equation are redefined as the probabilities of an increase or decrease in the population per unit time. This represents the unpredictability in natural populations of exact times between individual births and deaths. The random distribution applied to these probabilities is usually either the Poisson (number of state changes in a fixed time interval) or the negative exponential (time to next state change). These two distributions are used because they are memoryless; that is, the next state is dependent only on the present state and no other history is required. This choice of distribution matches the memoryless assumption present in ODE-based deterministic models.

Detailed examples of designing more complex SBD models are given in Donalson and Nisbet,[2] Renshaw,[6] Nisbet and Gurney,[7] and in the second part of this chapter. However, a brief example is useful

here. We look at a simple birth/death process whose deterministic representation is the ODE $dN(t)/dt = bN(t) - \delta N(t)$, where $N(t)$ is the total number of individuals at time t, b is the *per capita* growth rate, and δ is the *per capita* death rate. There are two possible state transitions in this process, $N \rightarrow N + 1$ and $N \rightarrow N - 1$. Because we are now dealing with a stochastic system, we redefine the rates as a set of probabilities. In a very small time interval $[t, t + \Delta t]$, the chance that there is a birth, $[N \rightarrow N + 1]$, is $bN(t)\,\Delta t$ and the chance of a death, $[N \rightarrow N - 1]$, is $\delta N(t)\,\Delta t$. Here we require that Δt be small enough that the chance of multiple state changes within the time interval be negligibly small. Alternately, instead of solving for ΔN, we can solve for Δt, the time to the next state change. The probability distribution of possible times to next event is then memoryless with mean $1/bN$ for $N \rightarrow N + 1$ and $1/\delta N$ for $N \rightarrow N - 1$. Law and Kelton[8] provide the formula for the memoryless distribution of possible times given a mean time as –ln(U[0,1])*mean where U[0,1] is a uniform random number generated between 0 and 1. In this example the stochastic time to next state transition is then the shorter of $-\ln(U[0,1]) * (1/bN)$ or $-\ln(U[0,1]) * (1/\delta N)$. Note that we can now simply advance from one state change to the next by calculating the two possible times to the next state change, advancing time to the shorter of the two times, and then executing the appropriate state change. This formulation is possible because these probabilities are independent of each other and of state changes at previous times. This is called a *continuous time* or *event-driven* model and is used in the construction of two of the four models described in this chapter. SBD models are only slightly more difficult to construct than deterministic models, but, because their predictions are probabilistic, one must also deal with statistical properties in their analysis.

Cellular automata (CA) are a class of models that relax the requirement that space be "well mixed" and allow explicitly for the presence, in some form, of individual entities. This class of models uses many of the same ideas as SBD models and is relatively easy to construct. Space is now included in the model explicitly as a grid of cells, and, unlike the ODE and SBD models, the focus of state changes is the individual cell as opposed to the population. The probability transitions described for the SBD model are applied to each cell with the added feature that the transition probabilities for the next state of a cell is not only dependent on its present state but also a function of the states of some set of its neighbors. Space is double-buffered meaning that there are actually two alternative cellular grids. One grid represents the present state and the other the next state. The next state for each cell in the present grid is recorded in the next state grid. When this is completed, the next state grid becomes the new present state grid, and the grid that was the present becomes the next state. Analyses of CA models are at a level of difficulty beyond that of SBD models because the effects of nonrandom spatial patterns may have to be included in analysis of the dynamics.

There are implicit assumptions regarding space and individuals in the CA class of models. A cellular array consists of a fixed number of locations. This means that, by default, in the special case of one individual per lattice site, the system has a carrying capacity that is equal to the number of cells. Because space consists of an array of cells, there is also fine-gained quantization of space. Thus, there is a minimum scale at which interactions can occur. Individuals are represented in their simplest form, just a set of discrete states.

Agent-based models (sometimes also referred to individual-based models) are a class of model that can, potentially, remove all implicit assumptions from the model structure. This class of model can be conveniently described in three parts: the agents, the infrastructure, and the interface (AI^2). The agents are typically the entities that comprise the populations of the state variables in a deterministic model. The infrastructure comprises the implementation of space and time. The interface is the system input and output, displays, internal data analysis procedures, etc.

There are two ways space can be represented in an ABM. Discrete space is similar to that of the CA model; however, the focus of interaction is now the individual, not the cell, so the cell now just represents some aspect of environmental space. Space can also be represented as continuous, where the position of an individual is represented by a real-valued X,Y coordinate pair. Time can be implemented as either discrete or continuous. In the case of continuous time, state transitions for individuals are inserted into or removed from a time-ordered event schedule, and, like the SBD, time is advanced from one event to the next. Because state transitions are now tied to the individual agent, the *per capita* rate as opposed to the total rate is used to calculate the time to state transition.

ABMs can be quite difficult to code and verify. In addition, given a result, deducing the contributions of the various underlying mechanisms is not trivial. In contrast, if we believe that individual behavior, in all its forms, is a contributing factor to population dynamics, this class of model must become part of the modeler's tool kit.

Each of the aforementioned class of models has strengths and weaknesses. On the gradient described earlier, as we move in the direction of more complex model classes, the ability to represent more complex interactions increases. However, the analysis of results and, in particular, the ability to isolate the relative strength of the contributions of the underlying mechanisms to the dynamic outcomes becomes far more difficult. Comparing and contrasting the results of different model classes can mitigate many of these problems. As discussed previously, each model class has some advantage of "realism" gained from removing an implicit assumption, with the negative trade-off of new technical challenges and more difficult analysis of results. We advocate multiple model analysis for two purposes, model *verification* and results *validation*, in a similar (but not identical) manner to Rykle.[9] Model verification is confirming that the code/equations that comprise the structure of the model are working as intended. We use the term *validation*, in its most general sense, to describe the analysis of the dynamic results once verification is completed. In general, a more complex model can be configured to match the implicit assumptions of a simpler model for the purposes of verification. Comparing the results of a simple model to a complex counterpart can validate or invalidate its use of implicit assumptions associated with the simpler model. And, using simpler models to factor out various mechanisms can help decompose complex results into the individual contributions of different mechanisms.

We now introduce an experimental system of mussels and their predators. We use the four previously described model classes to assist in our understanding of the dynamics of this system.

27.3 Mussels in the Intertidal Zone

The mussel *Mytilus californianus* is a dominant species of the intertidal zones of the North American continent. This species is found in narrow bands in shore sites of moderate to high wave exposure. The predators of *M. californianus* are the seastar, *Pisaster ochraceus*, in the Pacific Northwest,[10,11] and the spiny lobster, *Panulirus interruptus*, in Southern California.[12,13]

The ecology of mussel communities has been studied for over five decades. Early experiments suggested that the lower limits for *M. californianus* are set by predation and the upper limits are set by physical factors such as intolerance to dessication.[10,14] Thus, mussels experience a spatial refuge from predation at the upper intertidal zone. Paine[11] observed that below the upper intertidal zone there were patches of very large mussels that escape predation. This fact and the observation that seastars eat mussels smaller than the maximum available size suggested that mussels reach a certain size and become resistant to predation; this represents a "size refuge" hypothesis. More recent experiments emphasized supply-side effects,[15] suggesting that variation in recruitment rates is a source of variation in the adult populations, and recruitment produces feedback effects in the processes of competition and predation (see discussion in Robles and Desharnais[16]).

Later studies contradict the hypotheses of spatial and size refuges. In Southern California, time-lapse photography has revealed that spiny lobsters enter the upper intertidal zone at night and consume the mussels vertically along the shore.[12,17] Similar behavior was observed in the Pacific Northwest;[13] seastars move with the tides and are found foraging above lower boundaries of mussel beds. Also, experiments have shown that concentrations of adults mussels that occur above lower shore levels of the most wave exposed locations appear to result as much from the elevated rates of recruitment in these locations as from the impact of hydrodynamic stresses and tidal exposure on predator foraging.[18] It appears that the refuge hypothesis is an oversimplification of a more complex situation.

Mussel growth depends on the flow of water providing food, resulting in higher growth rates for mussels located lower in the intertidal zone and on wave-exposed shores.[19] The probability of being attacked by a predator decreases when a mussel is surrounded by larger mussels.[11,20–22] Thus, the rates of production and mortality in any specific location depend on the locations of a mussel in the gradients of tidal height and wave exposure and on the size and density of surrounding mussels. These observations

suggest the need for a new theoretical synthesis that will study rates of recruitment, growth, and predation mortality as a dynamic spatially explicit process.

We have developed a multiple-model approach to the study of predation in benthic communities. Four classes of models have been developed and analyzed, one from each previously discussed model class: (1) an analytical "mean field" approximation consisting of ODEs, (2) an SBD version of the mean field ODE model, (3) a CA model, and (4) an ABM. A set of model parameter values will be common to all four model types. Comparison and cross-validation can be made among models to take advantage of the strengths that each has to offer.

Our ODE model is based on the work of Nisbet et al.[23] where "space" is made up of a large number of very small "patches" that can be occupied by at most one mussel (algae in their model) and predators ("grazers" in their model) that move randomly among patches. Prey biomass grows in size in each patch until a predator grazes a patch to size zero. In Nisbet et al.,[23] as soon as grazers remove the algae from a patch there is algal regrowth. In our model each patch is either empty or occupied by a mussel. This model is given by a pair of differential equations:

$$\frac{\partial n(a,t)}{\partial t} = -\frac{\partial n(a,t)}{\partial a} - \mu(a,t)n(a,t), \tag{27.1}$$

$$\frac{dP(t)}{dt} = I - e_P(t)P(t), \tag{27.2}$$

where $n(a, t)$ is the density of prey of age a at time t and $P(t)$ is the density of predators. The first equation is the McKendrick–von Foerster model[24,25] for aging and death in an age-structured population where $\mu(a, t)$ is mortality rate for prey of age a at time t. We assume prey settle at a constant rate σ into empty patches, but the overall recruitment of prey decreases linearly until all available space is occupied at a maximum density K. This yields $n(0, t) = \sigma[1 - N(t)/K]$ as the boundary condition for new prey. In this open system, predators immigrate at the constant rate I and emigrate at the *per capita* rate $e_P(t)$, which may depend on the age and size structure of the prey population.

Prey size plays an important role in the predator–prey dynamics. We let $s(a)$ represent the size of a prey of age a and describe growth using the von Bertalanffy[26] formulation $s(a) = s_\infty - (s_\infty - s_0)e^{-\beta a}$, where β is the growth rate, s_∞ is the maximum size, and s_0 is the size of a newly settled recruit. We assume each prey's vulnerability to predation depends on its size and the density and size of prey in some spatial neighborhood of radius h surrounding the individual. In our mean field approximation, we assume that the size of the neighborhood $h = \infty$, and define $S(t) = \int s(a)n(a,t)da$ as the mean size of prey weighted by prey density. We write the mean field approximation for the per capita mortality rate of prey as $\mu(a,t) = \mu_0 + \theta P(t)e^{-cS(t)}$, which is independent of prey age but decreases exponentially with the weighted mean size of prey, $S(t)$. The parameter μ_0 is the mortality rate due to causes other than predation, θ is the predator attack rate, and c is a measure of how quickly resistance to predation increases with prey size. For predators, we assume that their emigration rate from the system is inversely proportional to the *per capita* rate of prey consumption; we use $e_P(t) = e_0[\theta e^{-cS(t)}]^{-1}$, where e_0 is the constant of proportionality relating prey consumption to predator emigration. Defining $N(t) = \int n(a,t)da$ as the overall prey density and taking the time derivative of $S(t)$, we can replace Equation 27.1 with a pair of ODEs yielding the system of three ODEs given in Table 27.1. (Details of this derivation are available in Desharnais et al., in preparation.) This system of equations is our ODE mean field approximation model.

The SBD model is a probabilistic version of the ODE model. Prey and predator densities are treated as discrete system variables. The dynamics are modeled as series of four possible transitions: the recruitment or death of a prey or the immigration or emigration of a predator. The time interval Δt between transitions is a continuous random variable chosen from a negative exponential probability distribution with an expected value that is the inverse of the transition rates. The transition rates follow from the ODE model.

Because it is a model of demographic stochasticity, the SBD forces us to consider the scale of the process being modeled. Transitions will occur much more frequently in a large system than in a small one. An additional parameter A must be used to represent the total size of the area being modeled. Since our system variables $N(t)$ and $P(t)$ are densities, the total numbers of prey and predators are $AN(t)$ and

TABLE 27.1

ODE and SBD Models and Parameters

ODE Model

State Variables	Equations
$S(t) \equiv$ weighted mean prey size (mm prey area^{-1})	$\frac{dS}{dt} = s_0\sigma + \left(s_\infty\beta - s_0\sigma K^{-1}\right)N(t) - \left(\beta + \mu_0 + \theta P(t)\, e^{-cS(t)}\right)S(t)$
$N(t) \equiv$ prey density (prey area^{-1})	$\frac{dN}{dt} = \sigma - \left(K^{-1}\sigma + \mu_0 + \theta P(t)e^{-cS(t)}\right)N(t)$
$P(t) \equiv$ predator density (predator area^{-1})	$\frac{dP}{dt} = I - e_0\left(\theta S(t)e^{-cS(t)}\right)^{-1}P(t)$

Stochastic Birth–Death Model

Transition	Transition Rate	State Changes
Prey recruitment	$A\sigma\left(\frac{K - N(t)}{K}\right)$	$N(t+\Delta t) = N(t) + A^{-1}$ $S(t+\Delta t) = S(t) + s_0A^{-1} + \Delta S$
Prey death	$A\left(\mu_0 + \theta P(t)e^{-cS(t)}\right)N(t)$	$N(t+\Delta t) = N(t) - A^{-1}$ $S(t+\Delta t) = \left(S(t) + \Delta S\right)\left(AN(t) - 1\right) / \left(AN(t)\right)$
Predator immigration	AI	$P(t+\Delta t) = P(t) + A^{-1}$ $S(t+\Delta t) = S(t) + \Delta S$
Predator emigration	$Ae_0\left(\theta S(t)e^{-cS(t)}\right)^{-1}P(t)$	$P(t+\Delta t) = P(t) - A^{-1}$ $S(t+\Delta t) = S(t) + \Delta S$
Prey growth	$\Delta S = \left(N(t)s_\infty - S(t)\right)\left(1 - e^{-\beta\Delta t}\right)$	

Model Parameters

Symbol	Definition	Default Values and Units
Area	Unit area (one "cell")	25 cm^2
A	Total system area	4×10^4 units of area
t	Time	1 day
a	Age	1 day
s	Prey recruitment rate	1 prey area^{-1} day^{-1}
s_0	Size of newly settled prey	1 mm
s_∞	Maximum prey size	200 mm
b	Decrease in prey growth rate with size	0.0004 day^{-1}
μ_0	Background *per capita* prey mortality rate	0.0001 day^{-1}
K	Maximum prey density	1 prey area^{-1}
q	Predator attack coefficient	1.0 unit area predator^{-1} day^{-1}
c	Resistance to predation with prey size	0.04 unit area mm^{-1}
I	Predator immigration rate	0.01 predator area^{-1} day^{-1}
e_0	Predator emigration constant	5.0 mm predator^{-1} day^{-2}

$AP(t)$, respectively. These quantities increase or decrease by one, or, equivalently, the variables $N(t)$ and $P(t)$ may increase or decrease by an amount A^{-1} at each transition. The transition rates are just the rates from the ODE model multiplied by A. The transitions and their rates are given in Table 27.1.

Prey growth presents a complication. Because size is a continuous variable, we must increment the system variable $S(t)$ by an amount that represents the growth of all prey during the time interval Δt. Fortunately, the von Bertalanffy growth model has the convenient property that if $s_i(t)$ is the size of an

individual *i* at time *t*, then the average size $\bar{s}(t)$ of all individuals follows the same growth equation as for a single individual: $\bar{s}(t+\Delta t) = s_\infty - \left(s_\infty - \bar{s}(t)\right)e^{-\beta\Delta t}$. Since $S(t)$ is mean size weighted by density, $S(t) = \bar{s}(t)N(t)$, and we obtain the expression for the increment ΔS due to growth given in Table 27.1. For a prey recruitment transition, we also add the size of the new recruit divided by the total area, s_0A^{-1}. Unlike the ABM, individuals are not tracked in an SBD, so for a prey death transition, we decrease $(S(t) + \Delta S)$ by an amount equivalent to the loss of one prey of average size; this amounts to multiplying by $(AN(t) - 1)/(AN(t))$.

Implementation of the SBD is fairly straightforward. A random time to the next transition is computed for each of the four possible transition types by generating a uniform random number, taking the negative of the natural logarithm, and dividing by the transition rate. The smallest of the four transition times determines Δt and the type of transition that occurs. Time is advanced to $t + \Delta t$ and the state variables are modified according to the transition rules. This process is repeated until a final simulation time is reached.

In the CA model space is represented explicitly as a rectangular grid of cells, where each cell has one unit of area and *A* is the total number of cells. Each cell represents a potential site of occupation by an individual prey. Because only one prey can occupy a cell at any time, we explicitly assume that there is no intraspecific competition for space among growing prey; an easily overlooked implicit assumption of the ODE and SBD models.

The recruitment, growth, and death of prey are modeled as transitions among "cell states." Each cell is denoted by its *x*,*y* coordinates in the grid and the state of a cell is represented by an discrete variable $S_{xy}(t)$. We use $S_{xy}(t) = 0$ to indicate an empty cell, $S_{xy}(t) = s_0$ for a cell with a new recruit, and $S_{xy}(t) = s_\cdot$ for a cell with a prey at the maximum size. The size range $[s_0, s_\cdot]$ is divided into *m* discrete increments, where *m* is chosen large enough to approximate continuous growth. Time is advanced in discrete steps Δt and all cell transitions occur simultaneously. Prey recruitment is represented as a transition from $S_{xy}(t) = 0$ to $S_{xy}(t + \Delta t) = s_0$. Prey growth is represented as a transition from $S_{xy}(t) = s$ to $S_{xy}(t + \Delta t) = s + \Delta s$, where $\Delta s \prod 0$. Prey death is represented as a transition from $S_{xy}(t) = s$ to $S_{xy}(t + \Delta t) = 0$ for $s > 0$. An additional "global variable" $P(t)$ represents the density of predators.

At each time step, cell transitions occur with probabilities that are derived using the rates specified in the ODE model (Table 27.1). For example, if Δt is sufficiently small, the probability that an empty cell will receive a recruit is given by $\sigma\Delta t$. Similarly, the probability that an occupied cell *x*,*y* becomes empty due to prey death is given by

$$\left(\mu_0 + \theta P(t)e^{-cS_{xy,h}(t)}\right)\Delta t\,,$$

where

$$S_{xy,h}(t) = (2h+1)^{-2}\sum_{i=x-h}^{x+h}\sum_{j=y-h}^{y+h} S_{ij}(t)$$

is the mean of the prey sizes in a neighborhood of $(2h + 1) \times (2h + 1)$ cells centered at *x*,*y*. (At the sides and corners of the lattice, $S_{xy,h}(t)$ is the mean of the subset of neighboring cells within the system.) If $h = 0$, then $S_{xy,0}(t) = S_{xy}(t)$ and the neighborhood is the cell *x*,*y* itself. When $h = \infty$, then $S_{xy,\infty}(t) = S(t)$ and we have the mean field approximation of the ODE and SBD models.

Prey growth is also treated as a stochastic process. For a prey of size *s*, the expected increase in size λ_s is given by the differential form of the von Bertalanffy model: $\lambda_s = \beta\left(s_\infty - s\right)\Delta t$. The expectation λ_s is then used as the mean parameter in a Poisson probability function to determine the actual increase in size Δs for each prey. In rare cases when $s + \Delta s > s_\infty$, we set $\Delta s = s_\infty - s$.

Predator immigration and emigration are treated as a random birth–death process. The number of predators that enter the system at each time step is chosen from a Poisson distribution with a mean value $AI\Delta t$. Each predator in the system at time *t* either leaves the system with probability $e_P(t)\Delta t$ or remains with probability $1 - e_P(t)\Delta t$. Assuming each predator makes its decision independently, we use a binomial distribution to determine the loss of predators. In the ODE model we assume that the *per capita* emigration rate $e_P(t)$ is inversely proportional to the predator's *per capita* consumption of prey. The same

assumption is used in the CA model, except the actual loss of prey biomass density to predators during the previous interval, $S_P(t)$, is computed by summing the sizes of the individual prey consumed by predators and dividing by the system area A. The emigration rate is then computed using $e_P(t) = e_0[P(t)\Delta t/S_P(t)]$, where the term in square brackets is the inverse of the *per capita* rate of prey consumption by predators. In rare cases when $S_P(t) = 0$, the probability that predators leave the system is set equal to one.

We use the AI^2 method to describe our ABM; however, as the interface is not germane to this discussion, it is not included.

In our ABM model, space is represented as a rectangle of area A. The boundaries are reflecting in the sense that predator movements are modeled as discrete jumps, but predators are not allowed to jump outside the system boundaries. (However, there is predator immigration into and emigration from the system across the boundaries.) The default space is continuous as opposed to the more common grid-based approach. Individuals are allowed to reside at any X,Y coordinate as opposed to the center of a grid cell.

State changes in the ABM model are tied to the individual. Each agent has a number of potential changes, such as feeding, death, or emigration. The times to each of these potential state changes are calculated using the *per capita* rates from the SBD model. All the times (with their associated individual and type of state change) are inserted into a time-ordered list called the event schedule. The next event (state change) is the one with the shortest time, which is also the event at the top of the list. As new individuals are added to the system their events are added to the event schedule, and, when an individual is removed from the system, any remaining events tied to that individual are removed from the event schedule. Finally, a predicted event associated with one individual can be altered by a change in another individual, thereby altering a previously scheduled event.

Mussels recruit at a constant rate σ, multiplied by the total area of the system A. New recruits are given a random X and Y pair of coordinates constrained to be within the system area and so that the initial diameter of the recruit will not overlap an edge. They recruit at size s_0 and are not allowed to overlap another individual. By default, if the coordinates of a new recruit overlap those of another individual, that recruitment is aborted and a new recruitment event is scheduled. There is also a configurable option that allows for multiple attempts to recruit a single individual by redrawing the coordinates a set number of times before aborting the attempt. Mussels are represented as circles and size is equivalent to the circle diameter. Note that, unlike the CA model, many small individuals can be packed into an area the size of one grid cell.

Mussels grow in the same manner as described for the SBD model. Because the ABM model uses continuous space, spatial competition must be included in the model. In the CA model, a grid cell has a diameter that is equal to the diameter of a full-grown mussel. As a result no two individuals can overlap. At most, two neighbors will just touch when both are at maximum size. With continuous space, this is not the case. Therefore, as a first cut at modeling spatial competition, we introduce the rule that no two individuals are allowed to overlap. At the point where two neighboring individuals just touch, they quit growing. The time at which this event occurs is computed explicitly from the von Bertalanffy equations and added to the event schedule. They remain at this size until either the individual dies or its neighbor dies. Upon the death of a constraining neighbor, an individual is allowed to resume growing. Death occurs from either background mortality as described in the CA model or from predation, as described later. Time to death from background mortality is chosen from a negative exponential distribution with mean $1/\_{0}$ and added to the event schedule at the time mussel is recruited.

Predatory seastars enter the system at a constant rate IA and are placed at random within the system boundaries. Unlike the mussels, overlap is allowed so no overlap check is necessary. All predators are assumed to be the same size and there is no predator growth. When the predator enters the system it is provided with a time in the future when it will leave the system using the equation $\frac{e_0}{\theta S(t)} e^{cS(t)}$ and calculated using the present system state. At that time, the individual is removed from the system, regardless of its location in space.

Seastars move randomly about the system in a series of jumps. Two random numbers $U[0,1]$ are generated. The first number is multiplied by the maximum distance that the predator is allowed to jump. (Note that a maximum jump distance close to the dimension of the system simulates a well-mixed

system, whereas a short jump distance allows for the possibility of local interactions affecting the system dynamics.) The second random number is multiplied by 2π to generate the direction in which the predator will move. The predator is then moved from its present position at the specified angle to the previously calculated distance. If this moves the predator off the map, then a new movement vector is chosen.

Each time a predator lands at a new location it searches an area the size of one unit of space. All mussels with centers that lie within this area are subject to attack. As with the CA model, the chance of a successful attack is a combination of the predators intrinsic ability to feed θ, modified by the protection provided by the mussel's own size and those of its neighbors, $e^{-cS(t)}$.

To match the CA model, it was necessary to add an additional configuration option to the ABM model. When an individual colonizes a grid cell in the CA model, it by default reserves the entire area of the grid cell for its use. This is in spite of the fact that at size s_0 it takes up only a very small part of the grid cell. To match this assumption, a grid-based cell array was overlaid on space. The rule that all individuals must "snap to" the center of each grid cell (the default discrete space requirement) and that only one mussel could occupy each grid cell was then applied to the system.

27.4 Examples of Model Verification and Validation

We now compare and contrast some basic results from each of our four models. Our analysis follows the general theme of this chapter. We first confirm that all models have the same basic behavior when all are configured with the same assumptions. We then look at some of the implicit assumptions inherent within each model and test them for robustness against the explicit results of a more complex model. We start by describing the dynamics expected from well-mixed large population using the ODE model.

The ODE model provides the baseline for our model analysis. The predicted dynamics of this model are summarized graphically in Figure 27.1. Setting $dP/dt = dN/dt = 0$, we can solve for the equilibria P^* and N^* in terms of S. Substituting these expressions into the equation for dS/dt and setting $dS/dt = 0$, one can show that the model equilibria are the real roots of the function $f(S) = s_0\sigma - (\beta + \mu_0)S - \kappa S^2 e^{-2cS} + \frac{K^{-1}\sigma(\beta s_\infty - \sigma s_0)}{K^{-1}\sigma + \mu_0 + \kappa S e^{-2cS}}$, $0 \le S \le s_\infty$, where $\kappa = I\theta^2/e_0$. This function is plotted in Figure 27.1A for the parameter values in Table 27.1 and three different rates of predation. In this case the model has two stable equilibria and one unstable equilibrium. At the stable equilibrium S_1^*, prey density and sizes are kept low by high levels of predation. At the stable equilibrium S_3^*, there is a high density of large prey that are resistant to predation. The unstable equilibrium S_2^* lies on a boundary separating the basins of attraction of the two stable equilibria. When predation rates are low, only the upper equilibrium S_3^* exists (Figure 27.1B). When predation rates are high, only the lower equilibrium S_1^* exists (Figure 27.1C). For biologically feasible parameter values such as those in Table 27.1, there is no evidence of exotic dynamics such as limit cycles or chaos.

Verification of the three stochastic models is demonstrated in Figure 27.2. In this case all three stochastic models were configured to match the implicit assumptions of the ODE model. We tested three elements here. The first is that the three stochastic models all converge to the same two stable equilibrium values as the ODE. The second is that all three stochastic models move to the correct stable equilibrium when they are started in that equilibrium's basin of attraction. Last, it is useful to note that, qualitatively, all the transient responses are similar.

There are two parts to our ODE validation. The first, testing the implicit assumption that demographic stochasticity can be discounted at a scale reasonable for our research, is demonstrated in Figure 27.3. Figure 27.3A shows ten realizations of the SBD model run at a system size that allows a total of 400 individuals ($A = 400$). Each run was started just above the unstable equilibrium (S_2^*) with a different random seed. As expected, the result is no longer deterministic, with three of the ten runs stabilizing at the lower equilibrium. Figure 27.3B shows the chance that the time series will stabilize at the upper equilibrium for a range of initial conditions about the unstable equilibrium for three different system sizes. The probability converges rapidly toward the prediction of the ODE model even at the relatively

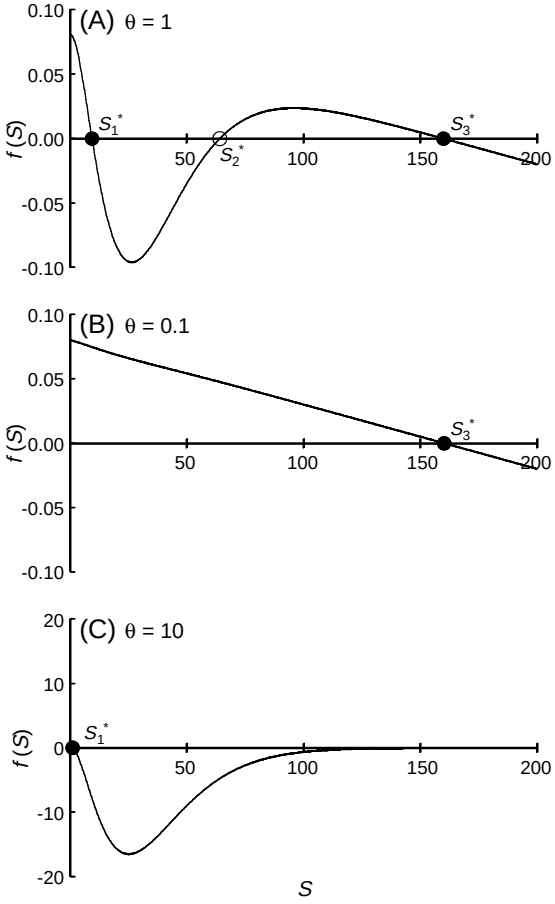

FIGURE 27.1 The ODE model predictions over a range of values of the predator attack coefficient, θ. The remaining parameters have the values given in Table 27.1. S_1^* is the lower stable equilibrium, S_2^* the middle unstable equilibrium, and S_3^* the upper stable equilibrium. (A) Two stable equilibria are present when the predator attack rate is at an intermediate value (θ = 1). (B) When the predator attack rate is low (θ = 0.1), only the upper stable equilibrium S_3^* exists. (C) When the predator attack rate is high (θ = 10), only the lower stable equilibrium S_3^* exists.

small system sizes used in this experiment. This indicates that demographic stochasticity should not have a significant effect on the steady state response at the default system size of A = 40,000 individuals (but see Donalson[27] and Harrison[28] for counter examples.) Figure 27.3C and D demonstrate a significant difference between the ODE and SBD, that is, the equilibria in the ODE are replaced by stationary probability distributions for the system variables in the SBD. In our case, this result is far more pronounced in the predator than the prey as demonstrated using the coefficient of variation (CV) of each time series (CV of prey is 0.043, CV of predator is 0.431.)

The ODE assumptions break down when space is not homogeneous and when individuals are not well mixed as shown in Figure 27.4. Figure 27.4A shows the mean field approximation for the neighborhood effect at the lower equilibrium. There is little evidence of any heterogeneity when the size protection for each mussel is calculated using the entire population ($h = \infty$). The same is true at the upper equilibrium (Figure 27.5B), with the exception that there is more variation in size among mussels. In contrast, when a mussel is protected by only its eight immediate neighbors (h = 1), occasionally a mussel escapes predation long enough to become too large for seastars to handle and it becomes the center of an "island" of protected individuals (Figure 27.4C). These islands can increase slowly in size and merge until the system resembles the upper equilibrium in Figure 27.4B. On the other hand, at the parameter values in Table 27.1, the ODE prediction of lower and upper stable equilibria holds well for moderate neighborhood

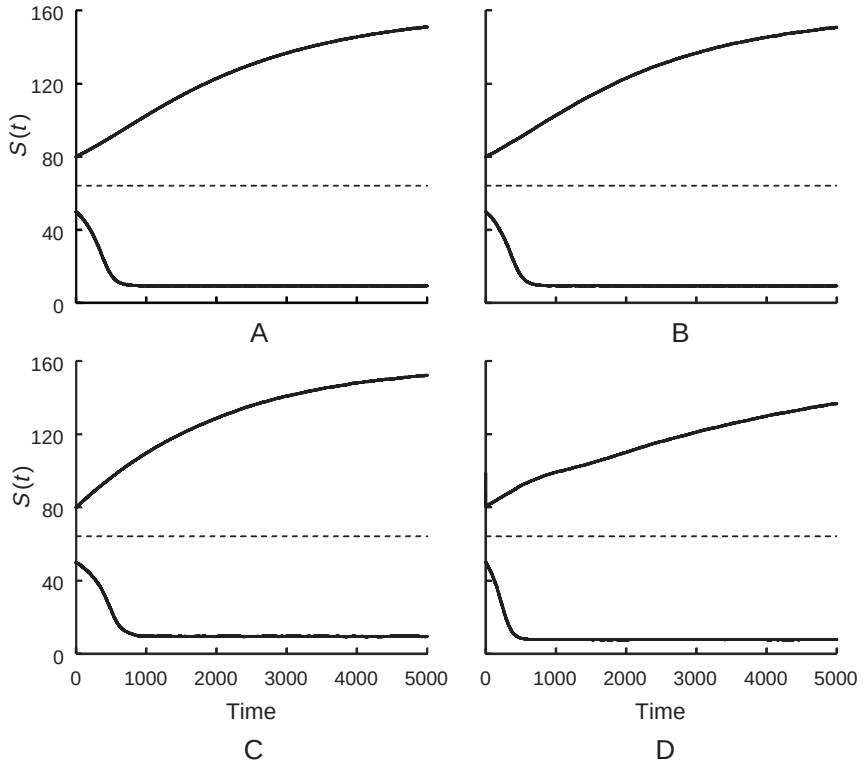

FIGURE 27.2 Two time series plots for each type of model. One plot starts at $S(0) = 50$ and the other at $S(0) = 80$. The dashed line is S_2^*. Time runs through $t = 5000$ days. All models were configured to match the implicit assumptions of the ODE model and used the default parameters from Table 27.1.

sizes of $h \prod 2$. Figure 27.4B and D show an interesting change in system dynamics when a continuous gradient is applied to space. Figure 27.4B shows the upper equilibrium with the default parameters. The distribution of sizes across space is random. In reality, seastars have more time to forage in areas that are submerged for longer periods during the tidal cycle. A simple representation of this is to assume a constant gradient of decreasing predator foraging rate starting in deep water and moving to the high tide mark. When a vertical gradient in the predation rate ($\theta = 2–0$) is applied to space, instead of a continuous change in the mussel sizes and density across space, we find a sharp transition from high density/large size to low density/small size. Given that, for our system, we believe that there are potentially both neighborhood effects from size protection and gradients in the predation rates, these results make it clear that neither the ODE nor SBD representations of our system alone will suffice for our modeling effort.

An implicit assumption of the CA model is that only one "individual" can occupy a single cell, regardless of the size of the individual. Figure 27.5 demonstrates the effect on the size distribution of individuals when this assumption of fine-grained spatial quantization, implicit in the CA model, is relaxed. Figure 27.5A shows a spatial plot of the ABM model at the upper equilibrium, configured to match the spatial assumptions of our CA model as described earlier in this chapter. Figure 27.5C is the size distribution of the spatial plot in Figure 27.5A. Figure 27.5B and D show the same results for the default continuous spatial configuration of the ABM model. There is a strong shift in the distribution of sizes between the two configurations. This is caused by a combination of continuous space and the requirement that individuals not overlap. Individuals can recruit into spaces that would be reserved for a single individual in a grid-based model. As the smaller individuals grow, they contact each other at a smaller size and stop growing. Interestingly, although the size distributions are significantly different between forms of the model, qualitatively, the dynamics between the two are similar. In particular, both forms of model exhibit two stable equilibria at low and high prey biomass.

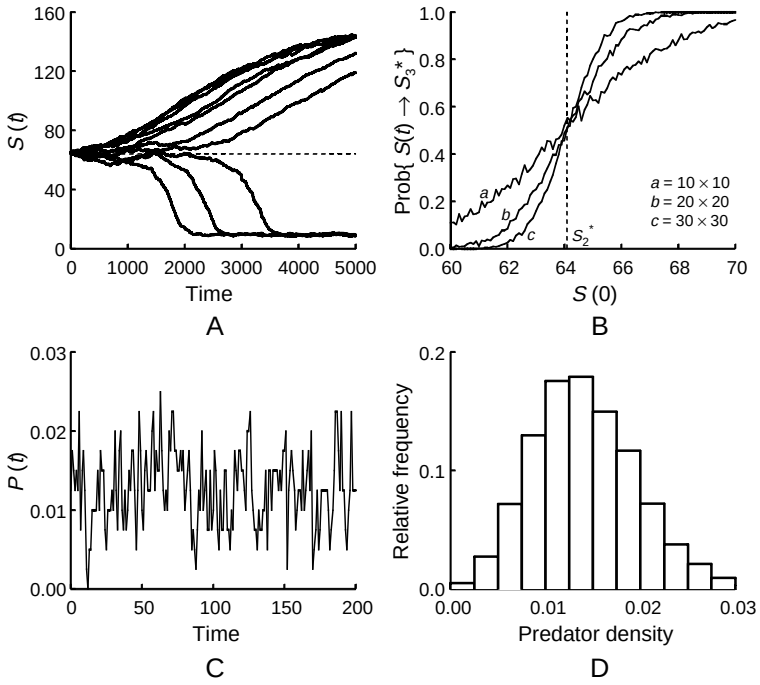

FIGURE 27.3 Results from the SBD model. (A) Ten realizations of the SBD with a 20×20 system started at $S(0) = 65$, which is just above the unstable equilibrium of $S_2^* = 64.1$ (dashed line). Three realizations go to the lower equilibrium and seven go to the upper equilibrium. (B) The effect of initial conditions and system size on the equilibrium; 1000 simulations were run at each of 100 initial conditions between $S(0) = 60$ and $S(0) = 70$ and the proportion that went to the upper equilibrium was computed. This experiment was repeated for three system sizes: (*a*)10×10, (*b*)20×20, and (*c*)30×30. The vertical dashed line locates the unstable equilibrium S_2^*. (C) A time series of predator density for a 20×20 system started at the lower equilibrium. (D) The frequency distribution of predator density for a 20×20 system started at the lower equilibrium and run for 5000 time units.

27.5 Discussion

It is certainly no small task to develop and analyze four different models of a single system. Why go to all this effort? The simplest route is to apply Occam's razor, that is, choose the simplest model. However, there is a caveat to that, it must be the simplest model that adequately represents the system. Therefore, for a simple model to be accepted, its results must be robust when its implicit assumptions are relaxed; otherwise the results are simply an artifact of the model class. On the other hand, a stand-alone complex model is very difficult both to test and to analyze. Without the support of simpler models, the results are problematic at best. However, when different models are combined, the results may be quite robust. There are two main lessons that we have learned from implementing a multiple-model approach. The first is that implicit assumptions in simple models are really explicit. The second is that building different models of the same process forces clearer understanding of the dynamics being represented.

We started with the assertion that models comprise two parts, the explicit assumptions, those that defined by the researcher, and the implicit assumptions, those set by the model class. In reality, an implicit assumption in a simple model class becomes an explicit assumption in a more complex model class. For all but the most complex model (the ABM model), we were able to configure a more complex model to match the implicit assumptions of a simpler model. Another way to look at this is that the set of all possible dynamics of a more complex model class is a superset of the set of all possible dynamics from a simpler model class. There has been much discussion in the ecological community on the possible errors introduced into complex models by introducing additional parameters that must be specified. The

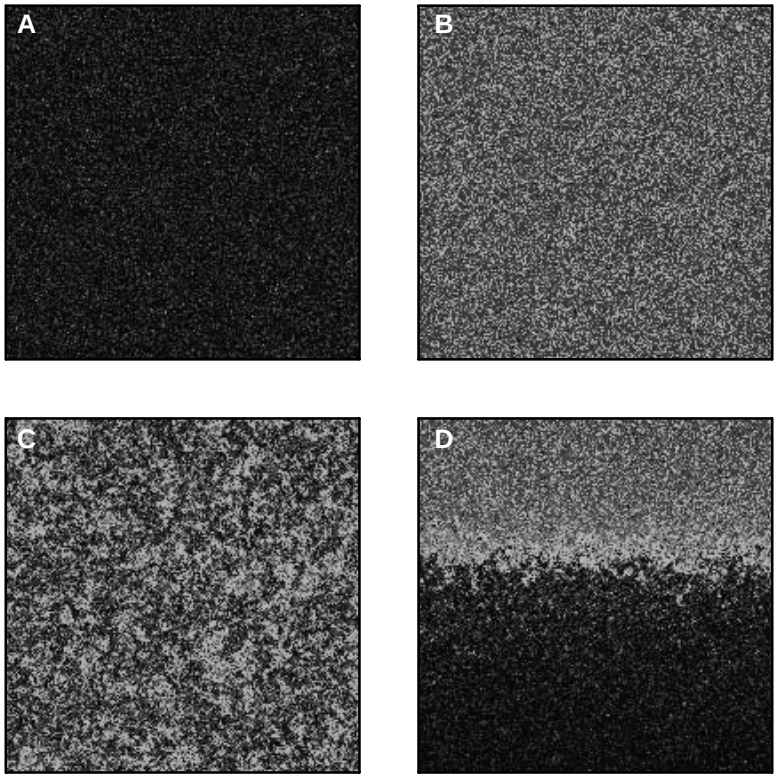

FIGURE 27.4 (Color figure follows p. xxx.) Two possible spatial effects are observed in the CA model when the mean field assumptions are relaxed. Each plot shows the size distribution of mussels over space, where mussel sizes are color-coded from blue for the smallest through red for the largest. The size distributions over space are shown for the mean field approximation ($h = \infty$) at (A) the lower and (B) the upper equilibria. (C) When the neighborhood size is small ($h = 1$) and the seastar attack rate is reduced ($\theta = 0.8$), "islands" of larger individuals develop at the lower equilibrium. (D) When a smooth linear gradient in the seastar attack rate is imposed from $\theta = 0$ at the upper boundary of the lattice to $\theta = 2$ at the lower boundary, and neighborhood effect is small ($h = 1$), the result is a sharp transition in prey cover similar to what is seen in many natural mussel beds. This predation gradient is what might be expected from differences in foraging times over the tidal height gradient.

argued solution has been to use a simpler model or model class. However, as was demonstrated above, the simpler model still contains an implicit representation of that parameter. Instead of at least an educated guess, the value is dictated solely by the assumptions implicit in that model class. It is reasonable to assume that setting a parameter implicitly may actually add greater error to a result that using an explicit but imperfect measurement of that parameter in a more complex model.

Perhaps the best reason for using multiple model classes to explore a system is that it forces researchers to understand the dynamics that they are attempting to simulate far better than if only a single model class were used. For example, imagine a model that includes logistic growth. Its representation in an ODE model is straightforward. Now imagine the same logistic growth function represented in an ABM. From the view of the individual what causes the suppression? Population number? If so, is it caused by the local or global population? Perhaps the phenomenon is triggered by lack of a resource such as food. Where in the life cycle does the density dependence occur? Mating could decrease, pregnancies could not come to term, or it could manifest in an increased death rate in a juvenile age class. These different possibilities can potentially have different effects on the dynamics of the population.

Within our research, comparing the continuous space ABM to the CA model forced detailed questions about how the individuals interact with one another and with space and led to the idea of implicit competition. Grid-based models by definition have a minimum scale for model interactions, the size of a single cell. An interesting consequence of this assumption occurs when using models where individuals

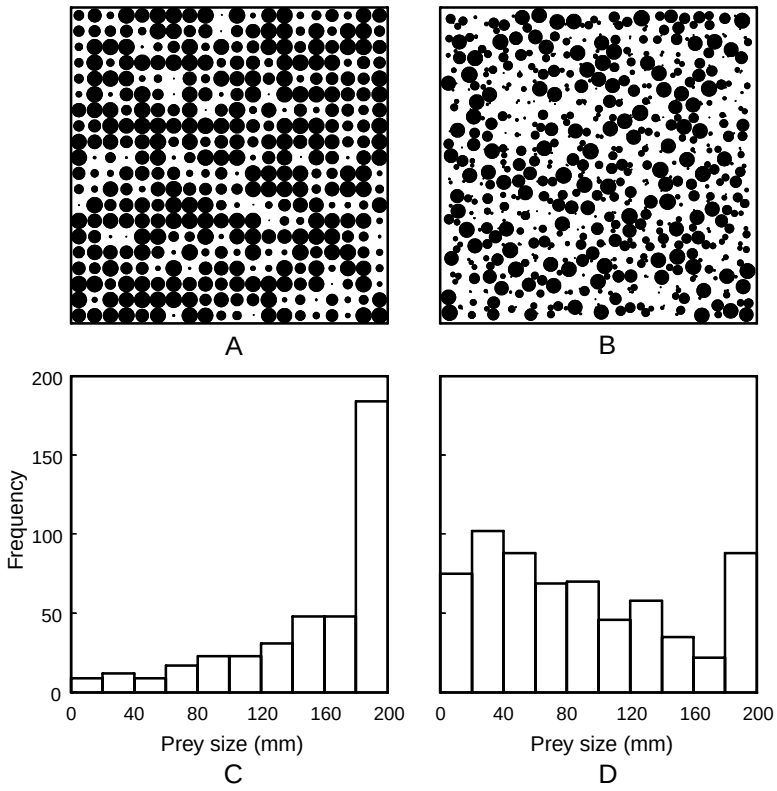

FIGURE 27.5 Results from the IBM model demonstrate the effects of using continuous space and allowing competition for space among mussels. The system size was 20×20 and the default parameters of Table 27.1 were used. The diameters of the filled circles are proportional to the sizes of the mussels. (A) The spatial distribution of mussels at the upper equilibrium for the mean field approximation when each prey is confined to a grid point. (B) The spatial distribution of mussels at the upper equilibrium for the mean field approximation when space is continuous and mussels grow until they touch another individual. The ODE prediction of a lower and upper stable equilibrium also holds when the assumption of grid-based space is relaxed. The histograms in (C) and (D) show the size distribution of mussels for the plots in (A) and (B).

have size as one of their attributes and only one individual is allowed per cell. When an individual colonizes a cell it preempts the entire area of the cell, even if it physically occupies only a very small portion of that area. This built-in spatial competition only became obvious to us when we were comparing the CA model to the ABM model.

As our research on the seastar/mussel dynamics has progressed, each of our four models has found its own niche. The ODE and SBD models will continue to be used as the deterministic and stochastic baselines for the rest of the model work. In particular we will be exploring different functional forms for phenomena such as size-dependent predation and neighborhood effects.

The CA model will be used to explore further the hypothesis that the abrupt lower boundary of mussel beds is a manifestation of two stable equilibria over smooth environmental gradients. The multiple equilibria hypothesis has already proved robust against demographic stochasticity (SBD), neighborhood effects (CA), and continuous space (ABM). Within the intertidal environment, we find fine-grained spatial heterogeneity such as boulders, underlying continuous gradients such as tidal height and wave exposure. One question that will be explored with the CA model is at what spatial scale will this spatial heterogeneity have an effect on the dynamics.

There are many assumptions within the ABM configuration. They occur either because this initial version of the ABM model is designed to match the simpler models or because it is necessary to have some starting point in any modeling project. Perhaps two of the most obvious assumptions are the emigration and immigration of the predators and the spatial competition among the prey. In the natural

system, predators enter and leave the system across a boundary. This implies two things. First, the immigration rate is dependent on the system perimeter as opposed to its area. Second, only individuals close to a boundary can choose to emigrate. A later phase of this research will explore the effect of these assumptions.

The spatial competition in currently used in this model is very restrictive. However, it was deemed the best starting point for the modeling task. There are other possibilities for modeling spatial competition among prey. Our current implementation permits only a monolayer of mussels. The other extreme is to allow complete overlap of the mussels. We have already developed a version of the ABM that has this assumption. However, it is clear that there is spatial competition within mussel beds. This and the fact that the other three models all use the no overlap assumption (the *K* value in the ODE and SBD models and the fixed number of cells in the CA model) argue against this configuration. A third possibility is to use layered space with a three-dimensional spatial model. This is a nontrivial task and will be attempted in a later stage of the research.

In this chapter we introduced the concept of applying multiple model classes to the analysis of a single system. The argument for this approach is that each model class brings with it both strengths and liabilities. Complex models are better suited for exploring interactions in space and time. However, they are hard to verify and analyze and tend to be slow. Simple models are easier to analyze and faster than their more complex counterparts, but they often require use of implicit assumptions that can significantly alter the resulting system dynamics. Comparing and contrasting the results of different model classes configured to simulate the same system can allow the researcher to tailor each model class to specific tasks that are optimized for that class. Although the multiple-model approach takes a greater investment in time over the short term, it provides more complete and robust results over the long term.

References

1. Holling, C.S. 1959. The components of predation as revealed by a study of small mammal predation of the European pine sawfly, *Can. Entomol.*, 91, 293–320.
2. Donalson, D.D. and R.M. Nisbet 1999. Population dynamics and spatial scale: effects of system size on population persistence. *Ecology,* 80, 2492–2507.
3. McCauley, E., W.G. Wilson, and A.M. De Roos, 1993. Dynamics of age-structured and spatially structured predator-prey interactions individual-based models and population-level formulations. *Am. Nat.,* 142, 412–442.
4. Wolff, W.F. 1988. Microinteractive predator–prey interactions, in W.F. Wolff, C.-J. Soeder, and F. Drepper, Eds., *Research Reports in Physics: Ecodynamics: Contributions to Theoretical Ecology: Proceedings of an International Workshop,* held at the Nuclear Research Centre, Julich, Fed. Rep. of Germany, 19–20 October 1987. Springer Verlag, New York, 285–308.
5. De Roos, A.M., E. McCauley; W.G. Wilson. 1991. Mobility versus density-limited predator–prey dynamics on different spatial scales. *Proc. R. Soc. Lond. B,* 246(1316), 117–122.
6. Renshaw, E. 1991. *Modeling Biological Populations in Time and Space*, Cambridge University Press, New York.
7. Nisbet, R.M. and Gurney, W.S.C. 1982. *Modelling Fluctuating Populations*. Wiley, Chichester, U.K.
8. Law, A.M. and W.D. Kelton. 1991. *Simulation Modeling and Analysis*. McGraw-Hill, New York.
9. Rykiel, E.J. 1996. Testing ecological models: the meaning of validation. *Ecol. Modelling,* 90, 229–244.
10. Paine, R.T. 1974. Intertidal community structure: experimental studies on the relationship between a dominant competitor and its principal predator. *Oecologia,* 15, 93–120.
11. Paine, R.T. 1976. Size limited predation: an observational and experimental approach with the *Mytilus-Pisaster* interaction. *Ecology,* 57, 858–873.
12. Robles, C.D. 1987. Predator foraging characteristics and prey population structure on a sheltered shore. *Ecology,* 68, 1502–1514.
13. Robles, C.D., R. Sherwood-Stephens, and M.A. Alvarado, 1995. Responses of a key intertidal predator to varying recruitment of its prey. *Ecology,* 76, 565–579

14. Connell, J.H. 1972. Community interactions on marine rocky intertidal shores. *Annu. Rev. Ecol. Syst.*, 3, 169–192.
15. Lewin, R. 1986. Supply-side ecology. *Science*, 234, 25–27.
16. Robles, C.D. and Desharnais, R.A. 2002. History and current development of a paradigm of predation in rocky intertidal communities. *Ecology* (in press).
17. Manly, B.F.J. 1993. Comments on design and analysis of multiple-choice feeding-preference experiments. *Oecologia*, 93, 149–152.
18. Robles, C.D., Alvarado, M.A., and Desharnais, R.A. 2001. The shifting balance of marine predation in regimes of hydrodynamic stress. *Oecologia*, 128, 142–152.
19. Dahlhoff, E.P. and B.A. Menge 1996. Influence of phytoplankton concentration and wave exposure on the ecophysiology of *Mytilus californianus*. *Mar. Ecol. Prog. Ser.*, 144, 97–107.
20. McClintock, J.B. and T.J. Robnett, Jr. 1986. Size selective predation by the asteroid *Pisaster ochraceous* on the bivalve *Mytilus californianus*, a cost benefit analysis. *Mar. Ecol.*, 7, 321–332.
21. Robles, C., Sweetnam, D.A., and Eminike, J. 1990. Lobster predation on mussels: shore-level differences in prey vulnerability and predator preference. *Ecology*, 71, 1564–1577.
22. Robles, C., Sherwood-Stephens, R., and Alvarado, M. 1995. Responses of a key intertidal predator to varying recruitment of its prey. *Ecology*, 76, 565–579.
23. Nisbet, R.M., S. Diehl, S.D. Cooper, W.G. Wilson, D.D. Donalson, and K. Kratz. 1997. Primary productivity gradients and short-tern population dynamics in open systems. *Ecol. Monogr.*, 67, 535–553.
24. A.G. McKendrick, 1926. Applications of mathematics to medical problems. *Proc. Edinburgh Math. Soc.*, 44, 98–130.
25. H. von Foerster, 1959. Some remarks on changing populations, in *The Kinetics of Cellular Proliferation*, Grune & Stratton, New York, 382–407.
26. Bertalanffy, L. von. 1938. A quantitative theory of organic growth. *Hum. Biol.*, 10, 181–213.
27. Donalson D.D. 2000. Modeling Complex Interactions: Theoretical Ecology Meets Pacman, Ph.D. dissertation, University of California at Santa Barbara, Santa Barbara, 2000.
28. Harrison, G.W. 1995. Comparing predator–prey models to Luckinbill's experiment with *Didinium* and *Paramecium*. *Ecology*, 76, 357–374.